Dalton Transactions

ROYAL SOCIETY OF CHEMISTRY

PAPER

View Article Online
View Journal | View Issue

Cite this: *Dalton Trans.*, 2022, **51**, 2385

Pseudotetrahedral Zn(II)-(*R* or *S*)-dihalogen-salicylaldiminato complexes with Λ- or Δ-chirality induction at-metal†

Hadi Amiri Rudbari, *[a] Arezoo Saadati,[a] Mahnaz Aryaeifar,[a] Olivier Blacque, [b] Isabel Correia, [c] Mohammad Khairul Islam, [d] Dennis Woschko, [e] Christoph Janiak *[e] and Mohammed Enamullah *[d]

Reactions of enantiopure (*S* or *R*)-*N*-1-(phenyl)ethyl-2,4-X^1,X^2-salicylaldimine (*S*-H or *R*-H; X^1, X^2 = dihalogen) with Zn(II)-nitrate give bis[(*S* or *R*)-*N*-1-(phenyl)ethyl-2,4-X^1,X^2-salicylaldiminato-κ^{2}N,O]-zinc(II), (Δ-Zn*S* or Λ-Zn*R*) with Δ/Λ-chirality induction at-metal in the C_2-symmetric molecules. EI-mass spectra show parent ion peaks. X-ray structures indicate that two phenolate-oxygen and two imine-nitrogen atoms from two molecules of the Schiff bases coordinate to the Zn(II) ion in a pseudotetrahedral geometry. Structural analyses give evidence that the *S*- or *R*-ligand chirality gives only one diastereomer Δ-Zn*S* or Λ-Zn*R* in an enantiopure crystal. Gas-phase optimized structures suggest that the Δ-Zn*S* or Λ-Zn*R* diastereomers are slightly more stable than Λ-Zn*S* or Δ-Zn*R* by 1–2 kcal mol^{-1}. The intramolecular interactions were analyzed with the Independent Gradient Model (IGM) using the program Multiwfn on the optimized structures and also indicate the diastereomeric preference of Δ-Zn*S*1 over Λ-Zn*S*1 (or Λ-Zn*R*1 over Δ-Zn*R*1). Variable time and temperature ^{1}H NMR spectra support the presence of only one diastereomer Λ-Zn*R* or Δ-Zn*S* in the bulk samples, backed by the simulated spectra which exhibit no diastereomerization in solution. In contrast, the reported Zn(II)-(*R* or *S*)-salicylaldiminato/naphthaldiminato complexes show a diastereomeric mixture of both Δ- and Λ-forms and a Δ ⇄ Λ equilibrium in solution. Electronic circular dichroism (ECD) spectra in solution display expected mirror-image relationships for the (*S* or *R*)-Schiff base ligands and the (*S* or *R*)-ligated complexes. Combined analyses of experimental and simulated ECD spectra further support the notion of diastereomeric excess of Δ-Zn*S* or Λ-Zn*R* in solution. The overall results thus suggest the preservation of chirality at-zinc induced by *S*- or *R*-ligands in a solid or solution. Supramolecular packing analyses explore different kinds of intermolecular interactions with the strongest one for X···O. Only the halogen atom in the *para* position is involved in these interactions with Br···O > Cl···O. Hirshfeld surface analyses also support these interactions between two molecules at a distance shorter than the sum of the vdW radii. Comparison of the experimental and simulated PXRD patterns from the single-crystal X-ray structures shows a good matching and confirms the phase purity of the bulk samples.

Received 15th December 2021,
Accepted 28th December 2021

DOI: 10.1039/d1dt04220c

rsc.li/dalton

[a]*Department of Chemistry, University of Isfahan, Isfahan 81746-73441, Iran. E-mail: hamiri1358@gmail.com*
[b]*Department of Chemistry, University of Zurich, Winterthurerstrasse 190, CH-8057 Zurich, Switzerland*
[c]*Centro de Química Estrutural, Instituto Superior Técnico, Universidade de Lisboa, Av Rovisco Pais, 1049-001 Lisboa, Portugal*
[d]*Department of Chemistry, Jahangirnagar University, Dhaka 1342, Bangladesh. E-mail: enamullah@juniv.edu*
[e]*Institut für Anorganische Chemie und Strukturchemie, Universität Düsseldorf, Universitätsstr. 1, D-40225 Düsseldorf, Germany. E-mail: janiak@uni-duesseldorf.de*

†Electronic supplementary information (ESI) available: Crystallographic data (Table S1); EI-mass spectra (Fig. S1); two-dimensional fingerprint plots (Fig. S2); Hirshfeld surfaces (Fig. S3); ^{1}H NMR spectra (Fig. S4 and S5); UV-Vis spectra (Fig. S6 and S7); Experimental ECD spectra for the Schiff bases and complexes (Fig. S8, S9a and b); DFT optimized structures (Fig. S10); simulated UV-Vis/ECD spectra (Fig. S11–S14); experimental and simulated ECD spectra (the opposite comparison) (Fig. S15). CCDC 2000644, 2000646, 2000648, 2000650, 2000652, and 2000653. For ESI and crystallographic data in CIF or other electronic format see DOI: 10.1039/d1dt04220c

Introduction

Achiral or chiral bidentate chelate ligands (A^A) induce metal-centered Δ/Λ-chirality in six-coordinated tris- or bis-chelate-metal complexes with an octahedral geometry.[1–10] This is due to an asymmetric arrangement of the ligands around the metal ion with D_3-symmetry in Δ/Λ-M(A^A)$_3$ or C_2-symmetry in Δ/Λ-M(A^A)$_2$(X$_2$). The bidentate chelate ligands (A^B) demonstrate the phenomenon in four-coordinated non-planar bis-chelate-metal complexes Δ/Λ-M(A^B)$_2$ with C_2-symmetry.[11–28] The use of asymmetric bidentate ligands with a chiral centre (*R*- or *S*-A^B) provides two diastereomers Δ-M(*R*-A^B)$_2$ and Λ-M(*R*-A^B)$_2$ {or Λ-M(*S*-A^B)$_2$ and Δ-M(*S*-A^B)$_2$} with one being thermodynamically preferred.[29–38] In fact, the thermo-

dynamics of intra- and intermolecular interactions controls Δ *vs.* Λ-chirality induction at-metal in *R*- or *S*-ligated complexes.[29–32,34–38] Therefore, experimental results in the solid and solution along with theoretical calculations reveal that the chirality induction at-metal can be phase dependent if the intramolecular interactions for Δ/Λ are very close in energy since the intermolecular interactions differ. Thus, a solvation-induced chirality inversion from Λ-Cu*R* or Δ-Cu*S* in the solid-state to Δ-Cu*R* or Λ-Cu*S* in solution (or gas phase structure calculations) was reported.[36,38] Inversion of metal centered chirality by solvent polarity or pH of the solution was reported in Ni/Ti/Re-complexes.[39–41] Similarly, a redox reaction (electron-transfer) induces chirality inversion at-metal in Co/Cu(II)-complexes.[42–44]

Our recent studies of X-ray structure determinations,[25,29–38] the most reliable and quantitative tools to assign the absolute configuration of the metal centre, suggest only the formation of a single diastereomer Λ-M(R-N,O)$_2$ or Δ-M(S-N,O)$_2$ in the enantiopure crystals of pseudotetrahedral [M(R or S-N,O)$_2$] (M = Co, Ni, Cu, and Zn; N,O = (Ar)-salicylaldiminato/naphthaldiminato[45,46]). Only in a single case, oppositely configured Δ-Cu(R-N,O)$_2$ or Λ-Cu(S-N,O)$_2$ is formed in Cu(II)-(Ar)-salicylaldiminate.[36] Examples of the co-existence of both diastereomers in a single crystal (*i.e.*, diastereomeric pair) are also reported.[17,30] However, the measurement of only one single-crystal structure, which is then usually reported as the only diastereomer found in the solid-state, does not exclude the existence of the other diastereomer (may be minor or major) in the bulk crystal sample as a diastereomeric mixture or conglomerate (if the two diastereomers crystallize separately). In this regard, differential scanning calorimetry (DSC) was used to check quantitatively and qualitatively for the existence of both diastereomers in bulk crystal samples which would manifest itself by showing two distinct phase transformation peaks.[29] The more intense peak would then correspond to the major diastereomer, while the less intense one belongs either to the diastereomeric pair (both Δ/Λ-M forms in a single crystal) or to the minor diastereomer in the case of a diastereomeric conglomerate.[29,44]

Due to various inter- and intra-molecular contacts, the preferred solid-state structures might not necessarily correspond to the thermodynamically stable diastereomer formed in the solution or gas phase. Indeed, concerning the existence of both diastereomers (be it equal or unequal amounts) or a single diastereomer in solution no conclusions should be drawn from the single-crystal structure determination but independent solution studies are necessary. The ^{1}H NMR spectra in solution can show two separate sets of signals associated with the Λ-M and Δ-M diastereomers (or a single set for Λ-M or Δ-M) and hence, provide quantitative information on diastereoselection and chirality induction for diamagnetic complexes.[29,33,37] Temperature and/or time dependent ^{1}H NMR studies may further demonstrate a dynamic equilibrium between the two diastereomers (*i.e.*, Λ-Zn ⇄ Δ-Zn).

Along with the experimental results, a thorough computational procedure by DFT/TDDFT was employed to understand and explain the diastereoselection phenomenon in detail. The optimized structures in the gas phase, in general, indicate the Λ-M*R* or Δ-M*S* diastereomers as relatively more stable than Δ-M*R* or Λ-M*S*, as in the solid-state structures[29–32,34–37] with only a few exceptions.[36,38] The excited state properties (UV-Vis/ECD spectra) were successfully used to assign the electronic/chiroptical properties, and to envisage qualitatively the diastereomeric description of the Λ- *vs.* Δ-form in *R*- or *S*-ligated complexes in solution. In fact, combined studies of experimental and calculated ECD spectra, in most cases, suggest the diastereomeric excess of Λ-M*R* or Δ-M*S* in solution, in parallel to the same diastereomer in the solid-state or the more stable calculated gas phase diastereomer.[25,29–32,34–37]

The previous results of metal(II)-(*R* or *S*)-(Ar)-salicylaldiminate/naphthaldiminate (metal = Co, Ni, Cu, Zn; Ar = C_6H_5, p-CH_3O/Cl/BrC_6H_4) reveal that the chirality induction at-metal is typically controlled by the ligand *R*- or *S*-chirality, which diastereoselectively gives Λ-M*R* or Δ-M*S* in the solid-state (in the investigated enantiopure single crystal) and in solution (or gas phase structure calculations),[25,29–35,37] with the exception of Δ-Cu*R* or Λ-Cu*S* in Cu(II)-(Ar)-salicylaldiminate in the solid-state.[36] Introduction of di-halogen substituents into the salicylal-ring in Cu(II)-(*S* or *R*)-*N*-1-(phenyl)ethyl-2,4-X^1,X^2-salicylaldiminate (X^1, X^2 = Cl, Cl/Br, Br/Cl, Br)[38] leads to the as usual formation of Λ-Cu*R* or Δ-Cu*S* in the solid-state, which however shows chirality inversion at-copper in the solution or calculated gas phase structures (*i.e.*, Δ-Cu*R* or Λ-Cu*S*). This chirality inversion is justified due to the solvation of the complexes in solution (*i.e.*, solute–solvent interactions). However, due to the paramagnetism of the Co/Ni/Cu complexes, no quantification by the ^{1}H NMR of the Λ-M and Δ-M diastereomeric ratio was available in solution.

This leads to the present investigation into the homoleptic Zn(II)-(*S* or *R*)-*N*-1-(phenyl)ethyl-2,4-X^1,X^2-salicylaldiminate with the formation of a single diastereomer as Λ-Zn*R* or Δ-Zn*S* in the solid-state. Single crystal X-ray diffraction measurements were carried out to elucidate the absolute configuration of the metal centre as Λ-Zn*R* or Δ-Zn*S*. Variable time and temperature ^{1}H NMR spectra (with simulation) were recorded to examine the presence of the Λ- and/or Δ-diastereomers or possible diastereomeric equilibrium (Λ ⇄ Δ) in solution. Electronic spectra (UV-Vis/ECD) and computational procedures were employed to rationalize the experimental results and to get insight into the electronic/chiroptical properties in solution. The supramolecular packing for the complexes was analyzed with the Hirshfeld surfaces using the program CrystalExplorer.

Results and discussion

Synthesis and characterization

The reactions of enantiopure (*S* or *R*)-1-phenylethylamine with 2-hydroxy-3,5-di-halogen salicylaldehyde provide the enantiopure Schiff base ligands (*S* or *R*)-*N*-1-(phenyl)ethyl-2,4-X^1,X^2-

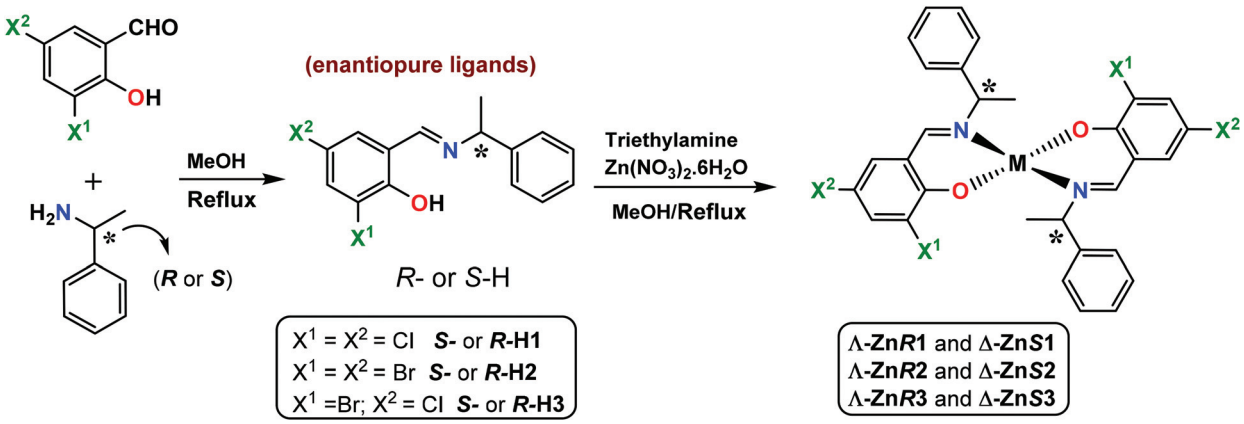

Scheme 1 Synthetic route to the formation of bis[(*S* or *R*)-*N*-1-(phenyl)ethyl-2,4-X^1,X^2-salicylaldiminato-κ^2N,O]-Λ/ΔZn(II), (Δ-Zn*S* or Λ-Zn*R*).

salicylaldimine {X^1, X^2 = Cl, Cl (*S*-H1 or *R*-H1); Br, Br (*S*-H2 or *R*-H2) and Cl, Br (*S*-H3 or *R*-H3}, which then react with Zn(II)-nitrate in the presence of triethylamine under reflux and give bis[(*S* or *R*)-*N*-1-(phenyl)ethyl-2,4-X^1,X^2-salicylaldiminato-κ^2N,O]-Λ/ΔZn(II), (Δ-Zn*S* or Λ-Zn*R*) (Scheme 1). The IR spectra for the complexes show very strong bands at 1611–1609 and 1584–1575 cm^{-1} due to the ν(C=N) and ν(C=C) stretching vibration, respectively. The EI-mass spectra display the parent ion peaks ([M = M(*S* or *R*)$_2$]$^+$) at *m*/*z* 650 for Zn*R*1 or Zn*S*1, 830 for Zn*R*2 or Zn*S*2 and 740 for Zn*R*3 or Zn*S*3 (Fig. S1†). The spectra also show the ion peaks at *m*/*z* 358 ([M(*S*1 or *R*1)]$^+$), 446 ([M(*S*2 or *R*2)]$^+$) and 402 ([M(*S*3 or *R*3)]$^+$) for the mono-ligated species of the complexes. The spectra further exhibit the ion peaks for the Schiff base ligands at *m*/*z* 292 ([*S*-H1–H or *R*-H1–H]$^+$), 383 ([*S*-H2 or *R*-H2]$^+$) and 339 ([*S*-H3 or *R*-H3]$^+$) and several ion peaks for the fragmented ligand species (see the Experimental section).

X-ray structural analyses

Molecular structures obtained from the single-crystal X-ray structures of the Zn(II)-Schiff base complexes are shown in Fig. 1 and the selected bond lengths and angles are given in Table 1. The complexes crystallize in non-centrosymmetric space groups (monoclinic, *I*2). The asymmetric unit contains half of the molecule that lies on a crystallographic 2-fold axis passing through the metal centre in all complexes. The metal ion is four-coordinated by two phenolate-oxygen and two imine-nitrogen atoms from two Schiff base ligands in a pseudotetrahedral geometry. Inspection of the metal–ligand bond distances reveals that the metal–oxygen bond is shorter than the metal–nitrogen bond, which indicates a stronger bonding interaction between the negatively charged oxygen anion and positively charged Zn(II) ion (Table 1).[16,19,20,29,37] The imine bond (C7–N1) distances are considerably small (1.280–1.285 Å), corresponding to a double bond character.[16,19,20,29,37]

Based on the structural data with very low absolute structure (Flack parameter)[47–50] values of 0.010–0.007 (Table S1†), for a given *R*- or *S*-ligand chirality only one diastereomer Λ-Zn*R* or Δ-Zn*S* is formed in the investigated (enantiopure) single crystal. The Δ- or Λ-configuration is induced diastereospecifically as a function of conformational preference of the N,O-chelate rings and/or the minimum steric requirements by the ligand substituents. These results are in agreement with the formation of Λ-M*R* or Δ-M*S* in the homoleptic Zn/Cu(II)-complexes[16,38] and the analogous M(II)-chiral-salicylaldiminato/naphthaldiminato (M = Co, Ni, Cu and Zn) complexes.[19,20,29–32,34,35,37] In contrast, oppositely configured Δ-M*R* or Λ-M*S* is formed in bis[(*R*)-*N*-1-(naphthyl)ethyl-3,5-dichloro-salicylaldiminato]-Δ-Zn(II)[20] or bis[(*R* or *S*)-*N*-1-(Ar) ethyl-salicylaldiminato]-Δ or Λ-Cu(II).[36] The opposite diastereomer in the latter Zn(II)-complex is due to the naphthyl group attached to the chiral-carbon center instead of the phenyl group in the present complexes (considering both *R*-forms).

The four-coordinated bis (N,O-chelate)zinc complexes distort somewhat from the tetrahedral geometry, as seen before.[16,20,29,37] The values of the degree of distortion, calculated from the dihedral angle (θ/°) or by using its normalized function ($\tau_{tet\text{-}sq}$ = θ/90°) or by using the geometry index τ_4,[29–32,51,52] are listed in Table S2,† and are similar for all Zn(II)-complexes (θ = 75.4–76.1°) irrespective of different substituents on the salicylal-ring, in parallel to the reported analogous Zn-naphthaldiminate (θ = 88.0–89.0°).[29] However, the degree of distortion is somewhat related to the substituents on the phenyl-ring attached to the chiral-carbon center in the Zn-salicylaldiminate (θ = 75.0–82.3°).[37]

Supramolecular packing analyses show different kinds of intermolecular interactions including X···H–C, X···O, X···π, X···M, H···C, H···O and H···H in all complexes (Fig. 2). Because of the halogen atoms as substituents on the Schiff bases, most of the strong intermolecular interactions are between the halogen and other atoms. Among these interactions, the strongest one is observed for X···O(1). It should be noted that only the halogens in the *para* position can be involved in the intermolecular halogen···oxygen interactions. From the X···O(1) interactions in Table S3,† the Br···O(1) interaction is the shortest and presumably strongest one. The van der Waals radii (vdW) for the Cl, Br and O atoms are 1.76, 1.87 and 1.58 Å, respectively, and the corresponding sums of the

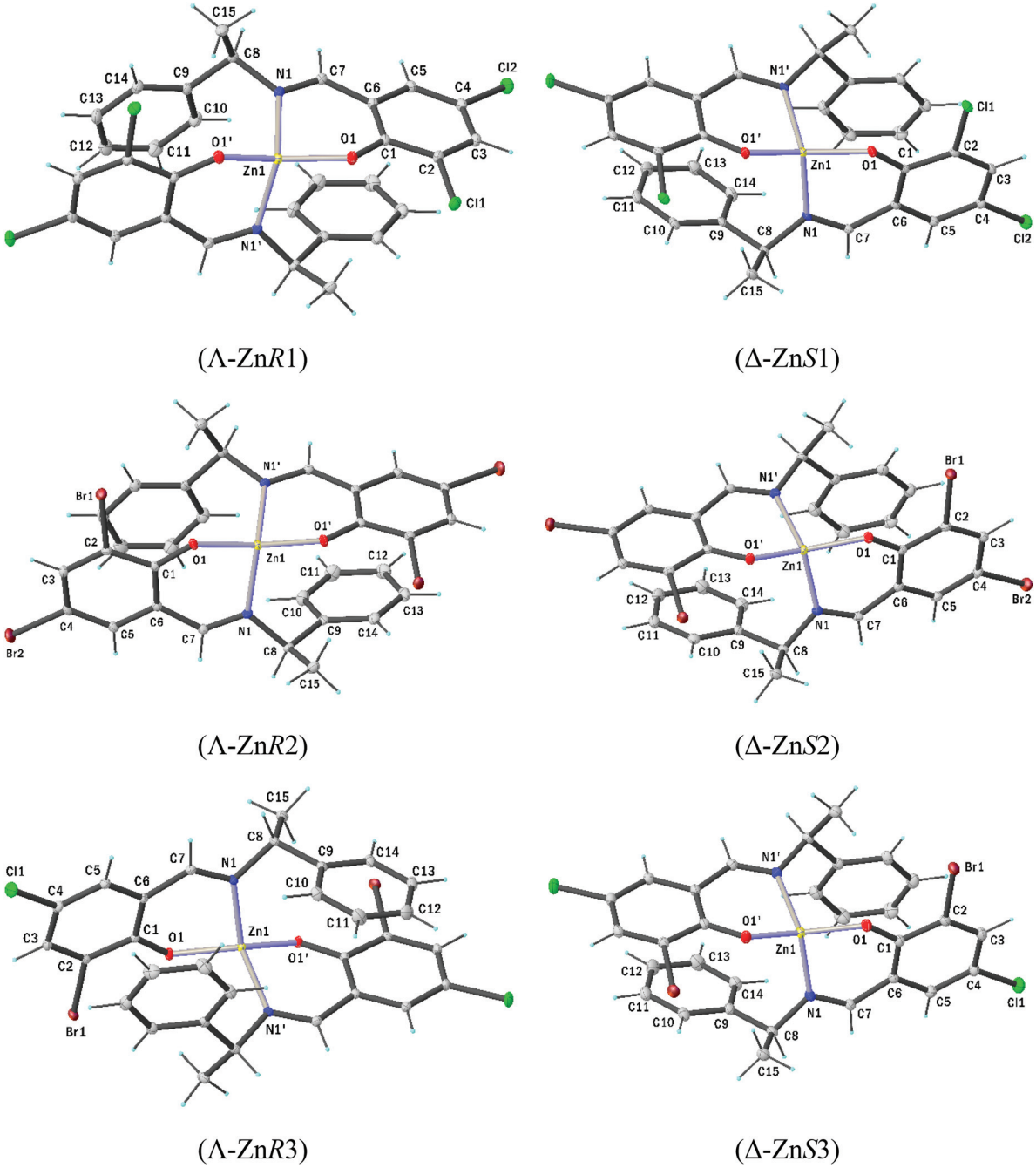

Fig. 1 Molecular structures for the enantiopure Zn(II)-chiral Schiff base complexes with Λ-Zn*R* and Δ-Zn*S* configurations in a pseudotetrahedral geometry. Thermal ellipsoids are drawn at the 30% probability level, while the hydrogen size is arbitrary (see Table 1 for bond length and angle values).

vdW radii are Cl + O = 3.34 and Br + O = 3.45 Å.[53] In conclusion, X···O(1) halogen bonding plays a more prominent role in the crystal packing of the complexes with the Br atom in the *para* position of the salicylal-ring as shown, for example, in Λ-Zn*R*2 (Fig. 3).

The X···π interaction is also another strong intermolecular interaction in the packing of the complexes. The geometrical parameters for the C–Cl···π and C–Br···π interactions are listed in Table S4.† In all complexes, the *ortho* halogen atom has an X···π interaction with neighboring molecules and *vice versa*. According to the geometric parameters in Table S4,† especially the r_b value that is slightly shorter than the sum of the van der Waals radii (vdW) of the halogen and carbon atom (*i.e.*, $r_C + r_{Cl}$ = 3.45 Å and $r_C + r_{Br}$ = 3.55 Å), these interactions can be categorized as strong localized (SL) interactions.[38,54]

Supramolecular packing in the crystals, as mentioned above, is further supported by the analyses of intermolecular

Table 1 Selected bond lengths (Å) and angles (°) for the Δ/Λ-Zn(II)-chiral Schiff base complexes

	Λ-Zn*R*1	Λ-Zn*R*2	Λ-Zn*R*3	Δ-Zn*S*1	Δ-Zn*S*2	Δ-Zn*S*3
Zn1–O1/O1′	1.9251(12)	1.9275(18)	1.926(2)	1.927(2)	1.928(2)	1.930(3)
Zn1–N1/N1′	2.0348(13)	2.038(2)	2.036(3)	2.036(3)	2.039(3)	2.039(3)
C7–N1	1.285(2)	1.282(3)	1.280(4)	1.281(4)	1.282(5)	1.282(5)
O1–Zn1–O1′	131.45(7)	131.98(12)	131.61(14)	131.37(13)	132.04(15)	131.59(17)
N1–Zn1–N1′	122.31(8)	121.64(13)	123.00(15)	122.11(15)	121.44(16)	122.95(18)
O1–Zn1–N1′	109.51(5)	109.25(8)	109.50(10)	109.62(10)	109.37(11)	109.45(11)
O1–Zn1–N1	93.59(5)	93.84(8)	93.28(10)	93.59(9)	93.77(11)	93.36(11)

Symmetry transformation used to generate equivalent atoms: ′ = 1 − *x*, +*y*, 1 − *z*.

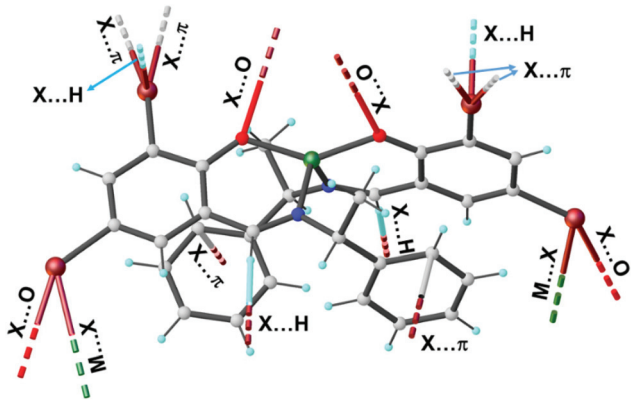

Fig. 2 Different intermolecular interactions: X···H–C, X···O, X···π, X···M, H···C, H···O and H···H in the crystal packing of Λ-Zn*R*2.

interactions with the Hirshfeld surfaces using the program CrystalExplorer.[55] The Hirshfeld surfaces with d_{norm} properties are illustrated in Fig. 4 and the fingerprint plots are shown in Fig. S2.† The percentages of contributions to various types of contacts in the fingerprint plots are summarized in Fig. S3.† The plots indicate that the highest contributions to the Hirshfeld surfaces are due to the H-atom interactions with other atoms such as carbon (H···C), halogen (H···X) and hydrogen (H···H). These three kinds of contacts contribute to more than 85% of the total Hirshfeld surface area of the complexes. Also, the chlorine and bromine intermolecular contacts (X···X, X···C, X···H, X···O and X···M) cover nearly 40% of the whole Hirshfeld surface (Fig. S3†). This can be attributed to the relatively large vdW radii of the halogen atoms. Hirshfeld surface analyses indicate the stronger intermolecular interactions between two molecules at a distance shorter than the sum of the vdW radii as red spots on the d_{norm} surfaces (Fig. 4). These strong intermolecular interactions are X···H, X···C, X···O and C···H, which cover nearly 61% of the whole Hirshfeld surface in all complexes (Fig. S3†). As we can see in Fig. S3,† halogen atoms exist in three of these four kinds of strong interactions (X···H, X···C and X···O), indicating their prominent role in crystal packing.

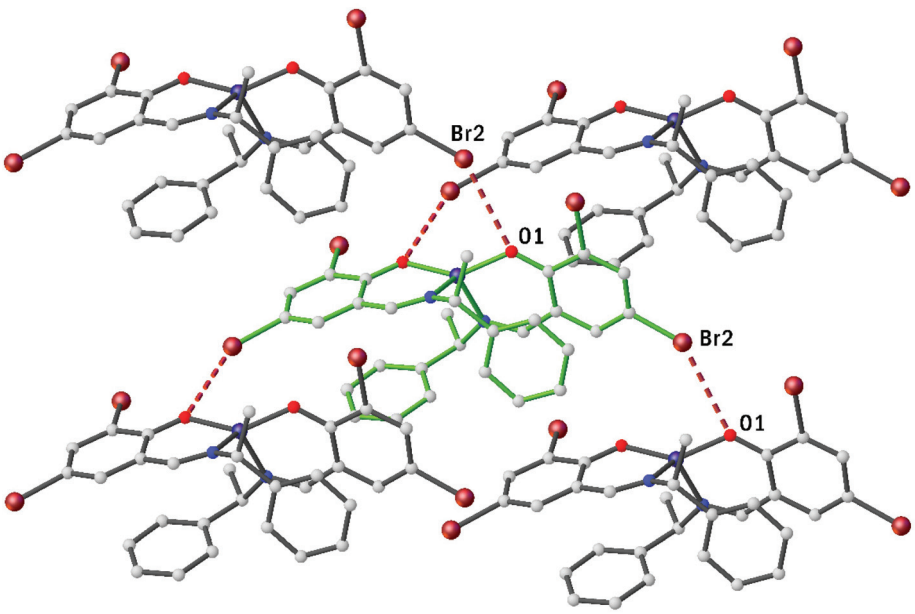

Fig. 3 Br···O(1) halogen bonding interactions in the crystal packing of Λ-Zn*R*2.

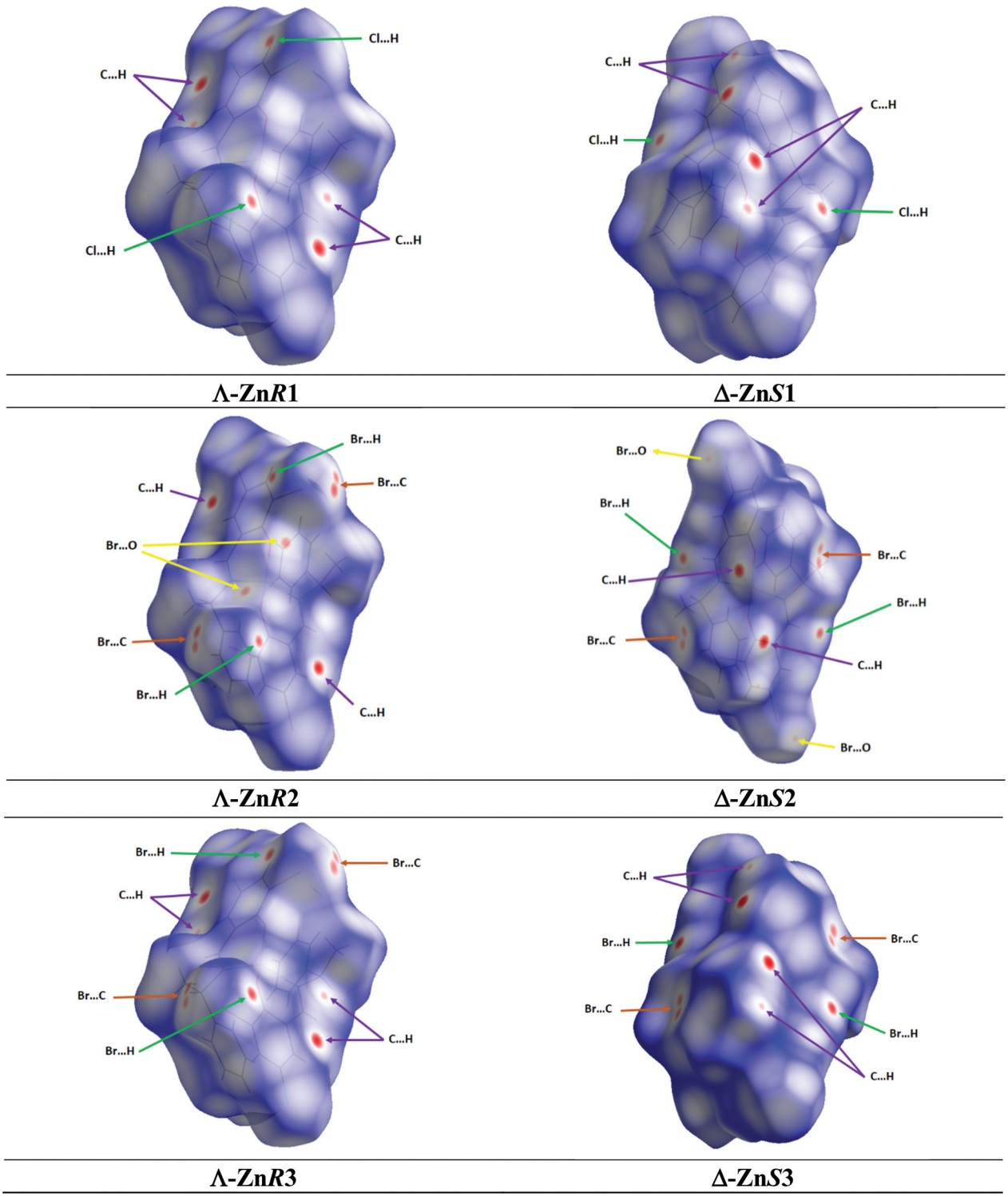

Fig. 4 Graphical illustration of the Hirshfeld surfaces with d_{norm} properties for the complexes. The strongest intermolecular contacts are shown in red color and weak contacts in blue color.

$^{1}H/^{13}C$ NMR spectra

The ^{1}H NMR spectra of the complexes in dmso-d_6 show several peaks for the coordinated Schiff base ligands to the metal ion (Fig. 5 and Table 2).[29,33,37,38] Each proton shows a well-separated peak at the upfield position in comparison with that in the free Schiff base ligands,[38] due to the formation of the complexes. The spectra show a doublet at *ca.* δ 1.46 ppm (J_{HH} = 6.8 Hz) for the methyl protons and a quartet at *ca.* δ 4.50 ppm for the methine proton. The imine proton appears as a most downfield singlet at

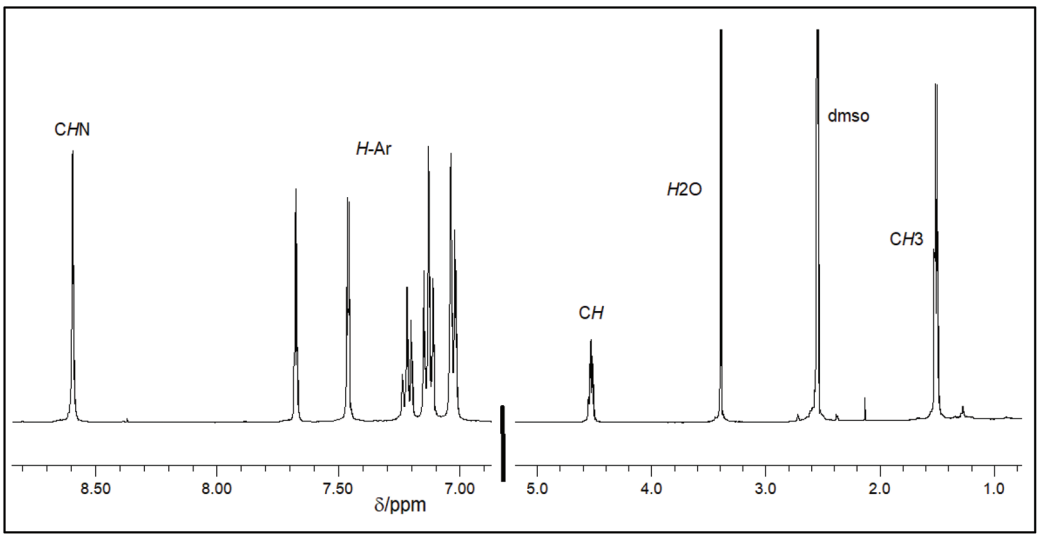

Fig. 5 ^{1}H NMR (400 MHz) spectrum for Zn*R*1 in dmso-d_6 at 25 °C (the single peak corresponds to the Λ-Zn*R*1 diastereomer in solution).

Table 2 ^{1}H/^{13}C NMR (400 MHz) spectral data for the Zn(II)-Schiff base complexes in dmso-d_6 at 25 °C

	^{1}H NMR			
Complexes	NC*H*	H_{Ar}	C*H*	CH_3
Zn*R*1 & Zn*S*1	8.54 (s, 1H) (8.38)[a]	7.62 (d, J_{HH} = 2.8 Hz, 1H); 7.41 (d, J_{HH} = 2.8 Hz, 1H); 7.17 (t, J_{HH} = 7.3 Hz, 1H); 7.08 (t, J_{HH} = 7.7 Hz, 2H); 6.98 (d, J_{HH} = 6.8 Hz, 2H)	4.47 (q, J_{HH} = 6.6 Hz, 1H) (4.43)[a]	1.46 (d, J_{HH} = 6.8 Hz, 3H)
Zn*R*2 & Zn*S*2	8.52 (s, 1H)	7.85 (d, J_{HH} = 2.1 Hz, 1H); 7.56 (d, J_{HH} = 2.1 Hz, 1H); 7.17 (t, J_{HH} = 7.2 Hz, 1H); 7.08 (t, J_{HH} = 7.5 Hz, 2H); 6.96 (d, J_{HH} = 7.3 Hz, 2H)	4.50 (q, J_{HH} = 6.5 Hz, 1H)	1.46 (d, J_{HH} = 6.5 Hz, 3H)
Zn*R*3 & Zn*S*3	8.52 (s, 1H)	7.87 (d, J_{HH} = 2.7 Hz, 1H); 7.45 (d, J_{HH} = 2.8 Hz, 1H); 7.17 (t, J_{HH} = 7.3 Hz, 1H); 7.08 (t, J_{HH} = 7.6 Hz, 2H); 6.96 (d, J_{HH} = 7.6 Hz, 2H)	4.50 (q, J_{HH} = 6.7 Hz, 1H)	1.47 (d, J_{HH} = 6.8 Hz, 3H)

	^{13}C NMR			
	NC*H*	C_{Ar}	C*H*	CH_3
Zn*R*1 & Zn*S*1	169.67	162.40, 140.47, 133.64, 133.12, 128.42, 127.80, 127.06, 126.45, 119.41, 116.31	67.28	20.99
Zn*R*2 & Zn*S*2	169.84	163.32, 140.58, 138.54, 137.50, 128.53, 127.86, 127.16, 120.09, 117.92, 103.63	67.42	21.21
Zn*R*3 & Zn*S*3	169.85	163.02, 140.54, 136.14, 134.47, 128.51, 127.84, 127.15, 119.17, 117.53, 116.96	67.42	21.22

[a] Calculated values for Λ-Zn*R*1 or Δ-Zn*S*1 at GIAO B3LYP/6-311+G(2d,p) with the PCM in dmso.

ca. δ 8.5 ppm, while several aromatic protons appear as doublets or triplets at δ 6.95–7.85 ppm. The spectra reveal no signal for the hydroxy proton (usually observed at δ 14.70–15.00 ppm in free Schiff base ligands[38]), confirming the deprotonation for the formation of the Zn–O bond during complexation. The ^{13}C NMR spectra exhibit several peaks associated with the coordinated Schiff base ligands,[38] as listed in Table 2.

A single set of signals for each proton suggests the presence of only one Δ- or Λ-diastereomer for each complex in solution, the more so as the single peaks are observed immediately (within *ca.* 5 min) after dissolution. Diastereomerization upon dissolution or a Δ/Λ-diastereomeric mixture in the bulk sample would give rise to two sets of signals for each proton, one set for each diastereomer. In accordance with the solid-state structures (*i.e.*, Δ-Zn*S* or Λ-Zn*R*), we assume that the observed single set of signals corresponds to the Δ-Zn*S* or Λ-Zn*R* diastereomer. These results are in contrast to those of Zn(II)-(*R* or *S*)-(Ar)-salicylaldiminate/naphthaldiminate[29,37] which showed two sets of signals for each proton, corresponding to the presence of both the Δ- and Λ-diastereomers in each complex in solution. The simulated ^{1}H NMR spectra, at GIAO B3LYP/6-311+G(2d,p) with the PCM in dmso, for the diastereomeric pairs Λ/Δ-Zn*R*1 or Δ/Λ-Zn*S*1 show a single signal for each proton in a single diastereomer. The results further reveal that the methine/imine protons are found at a higher field (*ca.* 4.43/8.38 ppm, very close to the experimental values, see Table 2) in Λ-Zn*R*1 or Δ-Zn*S*1, while at a lower field (*ca.* 5.52/8.56 ppm) in oppositely configured Δ-Zn*R*1 or Λ-Zn*S*1, as observed in the experimental ^{1}H NMR spectra for the analogous Zn complexes.[29,37] In addition, for a particular complex (Zn*R*1 or Zn*S*1), the chemical shift difference between the Λ- and Δ-diastereomers is *ca.* 1.10 ppm for the methine proton and 0.20 ppm for the imine proton, suggesting that the methine proton is significantly influenced by Λ *vs.* Δ-chirality

induction at-metal.[29,37] According to the reported Zn(II)-salicylaldiminato/naphthaldiminato complexes[29,37] and computational studies, where the bulk samples of the Zn complexes contain both the diastereomers, the ^{1}H NMR spectra would show two distinct sets of signals for each proton corresponding to the Λ- and Δ-forms in solution, which is not the case here in Fig. 5 and Fig. S4–S5† (Table 2). Although the stereochemical control may occur both in the solid and solution, the extent of the two phenomena differs from ligand to ligand. Hence, different behaviours in the two states might be observed by introducing different substituents into the chelating-ring. Thus in the case of the present Zn*R* or Zn*S* complexes, the experimental and computational results strongly suggest the existence of only one Λ- or Δ-diastereomer in solution, as in the solid-state, while different observations are reported in the analogous Zn(II)-salicylaldiminate/naphthaldiminate.[29,37]

The ^{1}H NMR spectra of the Zn(II)-chiral Schiff base complexes were successfully used for the quantitative and qualitative analyses of the Δ- and/or Λ-diastereomers or diastereomeric equilibrium (*i.e.*, in the case of a diastereomeric mixture) in solution as a function of variable temperature and/or time, provided that the Δ ⇄ Λ equilibrium is considerably slow in the context of a NMR time scale.[29,33,37] However, on ignoring NMR limitations (which may fail to show a very small amount of the diastereomer in the bulk samples or to detect a very fast Δ ⇄ Λ equilibrium, which gives the average as a single peak), the equilibrium can be easily followed based on the peak intensities for both the Δ- and Λ-diastereomers in solution. To check this equilibrium, we recorded the ^{1}H NMR spectra for Zn*R*2 with small amounts of the extra free ligand (*R*-H2) in dmso-d_6 at different time intervals (Fig. 6 and S4†). The spectra clearly show two sets of distinct peaks for the free Schiff base (*R*-H2)[38] and the complex (Zn*R*2), respectively. Here, the spectrum for Zn*R*2 again shows only one peak for each proton, corresponding to the Λ-Zn*R*2 diastereomer (as mentioned above). Thus, time dependent ^{1}H NMR spectra indicate no existence of the diastereomeric mixture or diastereomeric equilibrium even after 4 h of complex dissolution. Our previous report on bis[(*R*/*S*)-2-{(*E*)-(2-hydroxy-2-phenylethylimino)methyl}phenoxide-κ^{2}N,O]-Δ/Λ-Zn(II)[33] showed a diastereomeric equilibrium shift from a single diastereomer (100%, within 10 min of complex dissolution) to a diastereomeric mixture of 33/67 (within 40 min) or 46/54 (within 36 h) in $CDCl_3$. However, the present study results in a change in the peaks ratios for the free Schiff base to complex (*i.e.*, [*R*-H2]/[Zn*R*2]) with time. For example, the peak ratios for the methine or imine proton change from *ca.* 10/90 (immediately after complex dissolution) to *ca.* 25/75 (within 10 min), 50/50 (within 1 h) and 63/37 (within 4 h) in dmso-d_6, respectively (Fig. 6 and S4†). The results suggest the hydrolysis of the complex with time due to the presence of a small amount of water in dmso-d_6 which produces free Schiff bases, a very common feature of labile tetrahedral Zn(II)-complexes.[29,33,37]

The ^{1}H NMR spectra at room temperature (at 25 °C) show only one Δ- or Λ-diastereomer for each complex in solution, which means that another one may not be feasible due to thermodynamic instability or may be feasible at low temperature. Hence, to confirm the existence of both the Δ- and Λ-diastereomers or a single diastereomer (Δ or Λ), we recorded variable temperature (at 20, 0, −20, −30 and −40 °C) ^{1}H NMR spectra for Zn*R*1 in dmso-d_6/$CDCl_3$ (50%, v/v), respectively (Fig. S5†). The spectra show only one peak for each proton at all temperatures (also with the same peak intensity), indicating the presence of a single diastereomer Λ-Zn*R*1 (*i.e.*, no diaster-

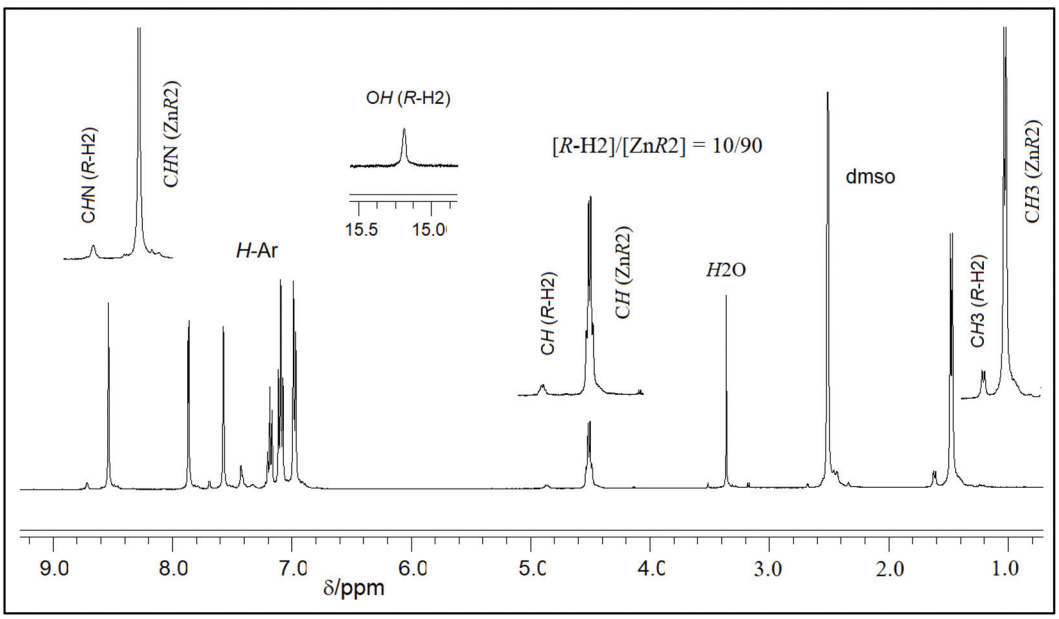

Fig. 6 ^{1}H NMR (400 MHz) spectra for Zn*R*2 containing small amounts of the extra free Schiff base (*R*-H2) in dmso-d_6 at 25 °C (immediately after complex dissolution). Peaks for Zn*R*2 and *R*-H2 are clearly and separately visible (the single peak for Zn*R*2 corresponds to the Λ-Zn*R*2 diastereomer only).

eomerization or a diastereomeric mixture, as discussed above). In contrast, the analogous Zn(II)-(*R* or *S*)-(Ar)-salicylaldiminate/naphthaldiminate[29,37] showed two distinct peaks for each proton, corresponding to a diastereomeric mixture of the Δ- and Λ-forms with an uneven ratio in solution. The equilibrium (Δ ⇄ Λ) shifts towards Λ-Zn*R* or Δ-Zn*S* at low temperature and Δ-Zn*R* or Λ-Zn*S* at high temperature. However, the variable temperature spectra (Fig. S5†) show several very weak peaks associated with the free Schiff base (<3.0%), resulting from the minor hydrolysis of the complex with time in solution.

Electronic spectra (UV-Vis and ECD)

The electronic (UV-Vis) spectra for the Schiff bases (Fig. S6†) and Zn(II)-Schiff base complexes (Fig. 7, S7†) are almost identical with a blue shift upon coordination to the metal ion. The spectra feature several bands/shoulders below 300 nm due to the intra-ligand π → π*/n → π* transitions (LL) and a relatively weak broad band at 300–450 nm due to the metal–ligand (ML) charge transfer transitions.[29,33,37] The electronic circular dichroism (ECD) spectra for the Schiff bases (Fig. S8†) and the complexes (Fig. 8, S9a and b†) show consistent similarities along the series, respectively. The ECD spectra feature several bands with opposite Cotton effects, associated with the different electronic transitions as shown in the UV-Vis spectra. The observed mirror-image relationships confirm the enantiopurity of the *S*- or *R*-Schiff bases and the diastereomeric excess of the Δ-Zn*S* or Λ-Zn*R* complexes in solution.[29–32,34–38] The ECD spectra show several bands for the *S*- or *R*-Schiff bases at: *ca.* 420 nm (+ or −, weak), 335 nm (+ or −, weak), 280 nm (− or +, very weak), 260 nm (+ or −, weak), 235 nm (− or +, weak), 220 nm (+ or −, weak) and 204 nm (− or +, very strong), respectively (sign, strength). Similarly, these bands are observed at slightly shifted positions in the Zn*S* or Zn*R* complexes at: *ca.* 400 nm (+ or −, strong), 365 nm (− or +, weak), 278 nm (− or +, strong), 255 nm (− or +, strong) and 240 nm (+or −, strong), respectively (Fig. 8, S9a and b†).

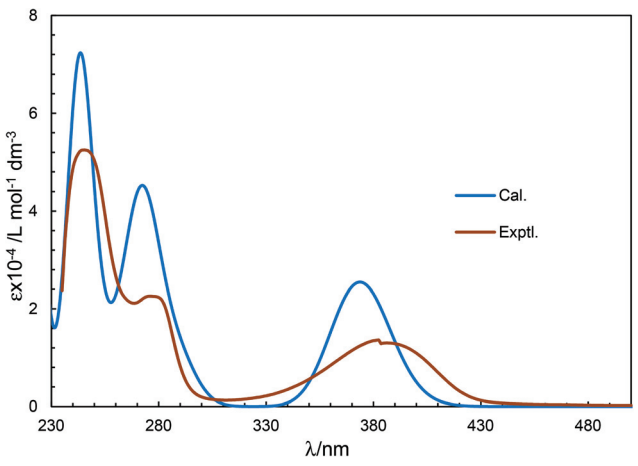

Fig. 7 Experimental UV-Vis spectrum for Zn*S*1 (3.22 × 10^{-2} mM) in methanol/chloroform (50%, v/v) at 25 °C and simulated spectrum (cal.) for Δ-Zn*S*1 at b3lyp/tzvp//b3lyp/6-31G(d) with the PCM in chloroform. The Gaussian band shape with exponential half-width σ = 0.16 eV.

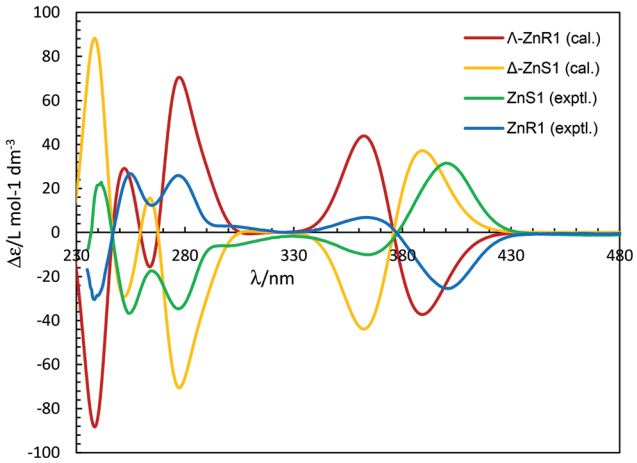

Fig. 8 Experimental and simulated ECD spectra for enantiomeric pair Zn*R*1/Zn*S*1 (*ca.* 3.00 × 10^{-2} mM) in methanol/chloroform (50%, v/v) at 25 °C ($\Delta\varepsilon_{exptl}$ values are increased by 2 times). Spectra simulated at b3lyp/tzvp//b3lyp/6-31G(d) with the PCM in chloroform, respectively. The Gaussian band shape with exponential half-width σ = 0.16 eV.

Optimized structures and excited state properties (Δ *vs.* Λ configurations)

The gas phase optimized structures for the diastereomeric pairs (*e.g.*, Λ-Zn*R*/Δ-Zn*R* or Δ-Zn*S*/Λ-Zn*S*) at b3lyp/6-31g(d) (Fig. S10†) show that the Λ-Zn*R* or Δ-Zn*S* diastereomers are slightly more stable than Δ-Zn*R* or Λ-Zn*S* by 1.0–2.0 kcal mol^{-1}. The metal centered chirality leading to the Δ- or Λ-configuration is induced diastereospecifically based on the conformational preference of the N,O-chelate rings and/or minimum steric requirements by the ligand substituents in the coordination sphere. The diastereoselectivity must originate from the intramolecular interactions between the ligands since the Zn complexes preserve the chirality also in solution. The optimized structures for the diastereomeric pair Δ-Zn*S*1/Λ-Zn*S*1 (Fig. S10†) were used for the analysis of the intramolecular interactions. The intramolecular interactions were analyzed with the Independent Gradient Model (IGM)[56] using the program Multiwfn (A Multifunctional Wavefunction Analyzer, Version 3.8(dev), release date: 2021-Nov-28).[57] The atom pair index $\delta g_{i,j}$ quantifies the contribution of the atom pair i and j to the interaction between two fragments (A and B with atom i being a part of fragment A and atom j a part of fragment B). The intrinsic bond strength index (IBSI) can be used to quantify the strength of chemical bonds and it may also be used to compare the strength of weak interactions.[58] The IBSI is defined in the framework of the independent gradient model (IGM). Based on the IBSI the program Multiwfn defined IBSIW (the IBSI for weak interaction) as follows.

$$\mathrm{IBSIW}(i,j) = 100 \times \frac{\delta g_{i,j}}{(d_{i,j})^2}$$

where $d_{i,j}$ is the distance between atoms i and j in Å. IBSIW has a somewhat better ability to distinguish the interaction strengths. The larger the IBSIW, the stronger the interaction.

In Multiwfn the δg index is given in a.u., and hence the formal unit of IBSIW should be a.u. $Å^{-2}$.

Each ligand in the Δ-Zn*S*1 and Λ-Zn*S*1 complexes was defined as a fragment and the 70 strongest inter-fragment (inter-ligand) interactions are listed in Table S5 for Δ-Zn*S*1 and Table S6 for Λ-Zn*S*1 (see the ESI†). It can be immediately seen that the sum of the IBSIW indices of these 70 strongest inter-ligand interactions is 22.09 a.u. $Å^{-2}$ in Δ-Zn*S*1 *versus* 17.56 a.u. $Å^{-2}$ in Λ-Zn*S*1. Hence the inter-ligand interactions are stronger in the experimentally found Δ-Zn*S*1 diastereomer. Table S7† compiles the sum of the related IBSIW indices for each atom in the fragment and thereby indicates the most strongly interacting atoms. Also included in Table S7 (ESI†) are the highest difference values between the Δ-Zn*S*1 and Λ-Zn*S*1 diastereomers. From Table S7† the sum of the IBSIW indices for Δ-Zn*S*1 (29.05 a.u. $Å^{-2}$) is significantly larger than that for Λ-Zn*S*1 (21.52 a.u. $Å^{-2}$). Note that in Table S7† all IBSIW indices are accounted for, while in Tables S5 and S6 (ESI†) only the 70 strongest ones are listed and summed up. Further analysis of the largest differences in these IBSIW indices Δ-Zn*S*1 − Λ-Zn*S*1 which are larger than ±0.50 helps to trace down the decisive interactions. Large differences are seen for the interactions of the methyl–C and –H atoms *versus* the methin(CH)–C and –H atoms. However, these differences are reciprocal in Δ-Zn*S*1 (stronger for CH_3) and Λ-Zn*S*1 (stronger for CH) and therefore will not explain the preference for Δ-Zn*S*1. Thus, the three next largest differences were analyzed and are listed in Table 3. Evidently, in the Δ-diastereomer one (Ph)C–H group and one salicyl C atom from each ligand can engage in stronger attractive interactions with the opposite ligand. From (Ph)C–H these interactions are primarily with the salicyl ring and can be described as C–H···π interactions (Table S8a and c, ESI†). In addition, there is a stronger (Ph)C–H···O interaction in the Δ-diastereomer. From the salicyl-C atom these interactions are π···H–C interactions with a (Ph)C–H group and with (CH_3)C–H (Table S8b, ESI†). Together, we see the sum of these weak intra-molecular interactions as decisive for the diastereomeric preference of Δ-Zn*S*1 over Λ-Zn*S*1. The analysis is, of course, identical for the respective enantiomeric forms Λ-Zn*R*1 over Δ-Zn*R*1.

The simulated UV-Vis spectra for each diastereomeric pair are essentially identical (Fig. S13†), while the ECD spectra show expected mirror-image relationships along the series (Fig. S14†). The resemblance of the experimental ECD spectrum to one of the simulated spectra (Λ-Zn or Δ-Zn) strongly suggests metal-centred Λ- or Δ-chirality, resulting from diastereoselection and chirality-induction in the *R*- or *S*-ligated complexes, respectively.[20,29–32,35–38] For metal-complexes with forbidden d–d transitions (as in the present case), the absolute configuration of the metal-centre is estimated from the metal–ligand and/or intra-ligand transitions in the ultra-violet or near ultra-violet region.[20,29,33,37] Thus, combined analyses of the ECD couplets in the experimental and simulated spectra allow us to assign the absolute configuration of the metal-centre. The present complexes, in parallel to analogous Zn(II) complexes,[20,29,33,37] show strong couplets at 330–430 nm (metal–ligand band) with −/+ or +/− signs for the *R*- or *S*-ligated complexes (Fig. 8, S9a and b†). Comparison of these couplets along with other couplets at a lower wavelength (230–300 nm), in the experimental and simulated spectra, indicates that the spectra for Zn*R* or Zn*S* are in good accord with the simulated spectra for the Λ-Zn*R* or Δ-Zn*S* diastereomer (Fig. 8, S9a and b†) (the opposite comparison for the Δ-Zn*R* or Λ-Zn*S* diastereomer is given in Fig. S15†). These results suggest that the ECD spectra for Zn*R* or Zn*S* correspond well to the diastereomeric excess of Λ-Zn*R* or Δ-Zn*S* in solution, resulting from diastereoselection and chirality induction at-metal.[29–32,35,38] Indeed, only the diastereomeric excess, that is an uneven mixture of Λ-Zn*R* and Δ-Zn*R* in solution, would give weak experimental bands with low $\Delta\varepsilon$ values – which is the case here in Fig. 8, S9a, b and S15.† Furthermore, variable temperature ECD spectra (from −40 to 80 °C) for the Zn-naphthaldiminato complexes[29] in solution showed that the band intensity increases upon cooling and decreases upon heating, while the overall band shape (exciton couplet) is well preserved. The intensity of the exciton couplets changes inversely with temperature and vanishes when an equilibrium mixture of Λ : Δ = 1 : 1 is reached (*i.e.*, no diastereomeric excess) at an estimated temperature of *ca.* 113 °C.[29]

Powder XRD studies

The PXRD patterns for all three pairs of complexes (Zn*R*1–3/Zn*S*1–3), measured over the 2θ range of 5–50° at ambient temperature, show consistent similarities for each pair and

Table 3 Sum of related IBSIW indices for atoms in the fragments in the Δ-ZnS1 and Λ-ZnS1 diastereomers with large differences[a] between Δ-ZnS1 and Λ-ZnS1 (except from Table S7, ESI)

	Δ-Zn*S*1		Λ-Zn*S*1		
Atom # in Frag 1, Frag 2[b]	Frag 1 IBSIW [a.u. $Å^{-2}$]	Frag 2 IBSIW [a.u. $Å^{-2}$]	Frag 1 IBSIW [a.u. $Å^{-2}$]	Frag 2 IBSIW [a.u. $Å^{-2}$]	IBSIW difference Δ-Zn*S*1 − Λ-Zn*S*1[c] [a.u. $Å^{-2}$]
(Ph)H 15, 47	3.067974	3.065524	1.371806	1.373200	1.70
(sal)C 1, 33	2.433725	2.433980	1.500074	1.499688	0.93
(Ph)C 14, 46	1.855479	1.855743	0.935916	0.936427	0.92

[a] Following the largest differences in the CH_3 and (methin)CH interactions, *cf.* Table S7 (ESI). [b] Fragment 1 is the ligand with atom numbers 1–31 and fragment 2 the ligand with atom numbers 33–63. See the graphs to Tables S5 and S6 (ESI) for atom numbering. [c] Rounded values and the average from the differences between fragment 1 and fragment 2, respectively.

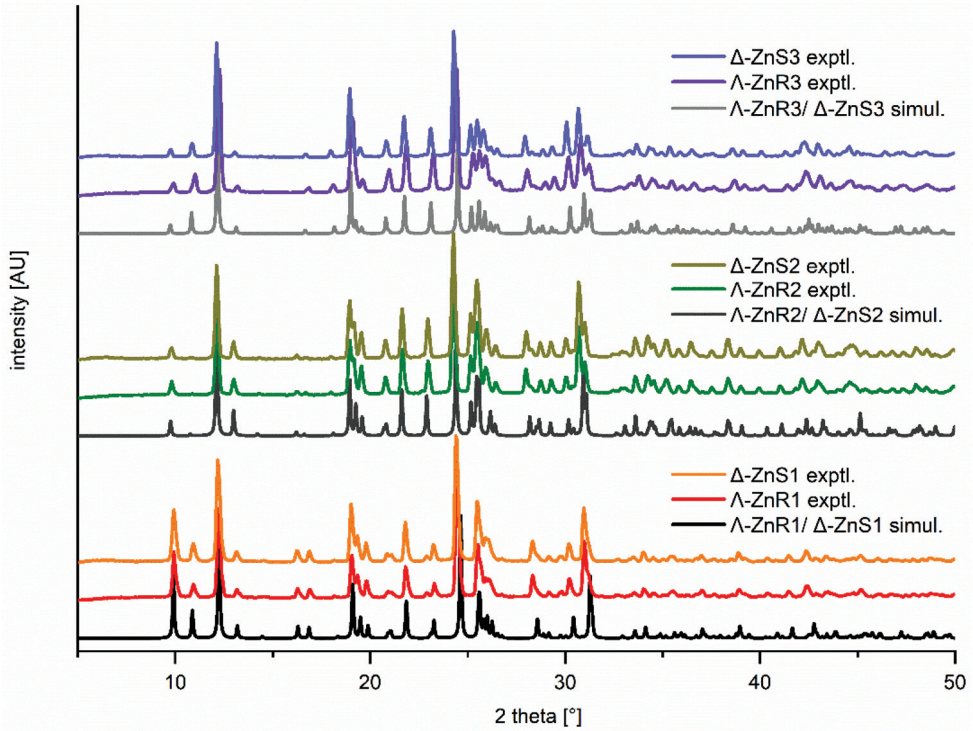

Fig. 9 Experimental and simulated PXRD patterns for all three pairs of complexes (Zn*R*1–3 and Zn*S*1–3) at ambient temperature.

along the series (Fig. 9). Comparison of the experimental PXRD patterns with the simulated patterns from the single crystal X-ray structures reveals a fair matching and hence, confirms the phase purity of the bulk samples of the complexes.

Conclusion

The X-ray molecular structures of bis[(*S* or *R*)-*N*-1-(phenyl) ethyl-2,4-X^1,X^2-salicylaldiminato-κ^{2}N,O]-Δ- or Λ-Zn(II) refer to the formation of the Δ-Zn*S* or Λ-Zn*R* diastereomer with chirality-induction at-metal in a pseudotetrahedral C_2-symmetric geometry. Analysis of the intramolecular interactions on the optimized structures also indicates the diastereomeric preference of Δ-Zn*S*1 over ΛZn*S*1 (or Λ-Zn*R*1 over Δ-Zn*R*1). The ^{1}H NMR studies along with simulation also show a single diastereomer Δ-Zn*S* or Λ-Zn*R* and no sign of diastereomerization in solution. In contrast, the reported analogous Zn(II)-(*R* or *S*)-salicylaldiminato/naphthaldiminato complexes exhibited a diastereomeric mixture of Δ- and Λ-Zn*S* (or Λ- and Δ-Zn*R*) with an equilibrium (Δ ⇄ Λ) shift in solution. The ECD spectra in solution display mirror-image relationships, suggesting the enantiomeric excess of the *S*- or *R*-Schiff base ligands and the diastereomeric excess of Δ-Zn*S* or Λ-Zn*R*, supported by the combined analyses of the experimental and simulated spectra. The results thus signal a preservation of chirality-induction at-zinc in the solid and in solution. Crystal packing and Hirshfeld surface analyses display different kinds of intermolecular interactions with the strongest one for X···O at a distance shorter than the sum of the vdW radii. The halogen atom in the *para* position is involved in these interactions with the sequence of Br···O > Cl···O. The present results manifest that the diastereoselection and Λ/Δ-chirality induction at-metal are significantly influenced by the metal-ion selection and the substituents on the chelating-ring in addition to, in general, the preference by the ligand chirality alone.

Materials and methods

$Zn(NO_3)_2{\cdot}6H_2O$, 3,5-dibromosalicylaldehyde, 3,5-dichlorosalicylaldehyde, 3-bromo-5-chlorosalicylaldehyde, (*R*)-(+)-α-methylbenzylamine and (*S*)-(−)-α-methylbenzylamine were obtained from Sigma-Aldrich and used without further purification. IR spectra were recorded on a Nicolet iS10 spectrometer at ambient temperature. EI-MS: Thermo-Finnigan TSQ 700. Isotopic distribution patterns for combined $^{64/66}$Zn + $^{35/37}$Cl and/or $^{79/81}$Br containing ions are clearly visible in the mass spectra. Peaks were observed due to the highest natural abundance of the isotopes. ^{1}H/^{13}C NMR spectra were recorded on a Bruker Avance III 400 spectrometer using dmso-d_6 as the solvent at 25 °C. ^{1}H NMR spectra were recorded at different temperatures (*i.e.*, 0, 20, −20, −30 and −40 °C) in dmso-d_6/$CDCl_3$ (50%, v/v), and at different time intervals in dmso-d_6 at 25 °C. Elemental analysis was performed on Leco, CHNS-932 and PerkinElmer 7300 DV elemental analyzers. UV-Visible spectra were recorded with a Shimadzu UV 1800 spectrophotometer in methanol/chloroform (50%, v/v) at 25 °C. Electronic

circular dichroism (ECD) spectra were recorded on a Jasco J-720 spectropolarimeter in methanol/chloroform (50%, v/v) at 25 °C. PXRD patterns for all three pairs of complexes were collected with a Bruker D2 Phaser powder diffractometer over a 2θ range of 5–50° on a flat silicon, low background sample holder at 30 kV, 10 mA with Cu-Kα radiation (λ = 1.5418 Å) for 30 min at ambient temperature. The most intense reflection in each diffractogram has been normalized to 1 and matched with the simulated PXRD patterns calculated with the MERCURY 2020.3.0 software.[59]

Synthesis of the complexes

A methanol solution (10 mL) of enantiopure (*R* or *S*)-1-phenylethylamine (5 mmol) was added dropwise to a methanol solution (10 mL) of 2-hydroxy-3,5-halogen salicylaldehyde (5 mmol). After being continuously stirred for 2 h in reflux, a solution of triethylamine (7 mmol) in methanol (5 ml) was added into this solution. The mixture was stirred for 10 min and then a solution of $Zn(NO_3)_2{\cdot}6H_2O$ (2.5 mmol) in methanol (10 mL) was added. Immediate precipitation of the complex occurred upon addition of the zinc salt. The resulting solution was refluxed for further 4 h. The yellow microcrystals of bis[(*S* or *R*)-*N*-1-(phenyl)ethyl-2,4-X^1,X^2-salicylaldiminato-κ^{2}N,O]-zinc (II), (Zn*R*1–3 or Zn*S*1–3) were isolated from the solution and purified by washing with cold methanol (1 mL) 3 times. Suitable single crystals for X-ray crystallography were obtained *via* slow evaporation of a concentrated solution of the complexes in methanol/chloroform (50%, v/v) at room temperature after 3–4 days.

Bis[(*R*)-*N*-1-(phenyl)ethyl-2,4-Cl,Cl-salicylaldiminato-κ^{2}N,O]-zinc(II) (Zn*R*1). Yield: 88%. IR (KBr, cm^{-1}): ν = 3064, 3034, 2979, 2937w (H–Ar), 1611vs (C=N), and 1575sh (C=C). MS (EI, 220 °C): *m*/*z* (%) = 650 (8) [M = $Zn(R1)_2]^+$, 545 (2) [M–CH$(CH_3)(C_6H_5)]^+$, 476 (4) [M–CH$(CH_3)(C_6H_5)$–2Cl + H]$^+$, 358 (7) [M$(R1)]^+$, 292 (19) [*R*-H1−H]$^+$, 189 (12) [$C_6H_2(Cl_2)$(CHNH)(OH)]$^+$, 105 (100) [C_6H_5(CHNH)]$^+$ and 77 (14) [$C_6H_5]^+$ {*R*-H1 = $C_{15}H_{12}Cl_2NOH$ = (*R*)-*N*-1-(phenyl)ethyl-2,4-Cl,Cl-salicylaldimine}. Anal. calc. for $C_{30}H_{24}Cl_4ZnN_2O_2$: C, 55.29; H, 3.71; N, 4.30%. Found: C, 55.31; H, 3.70; N, 4.28%.

Bis[(*S*)-*N*-1-(phenyl)ethyl-2,4-Cl,Cl-salicylaldiminato-κ^{2}N,O]-zinc(II), (Zn*S*1). Yield: 86%. IR (KBr, cm^{-1}): ν = 3064, 3034, 2979, 2937w (H–Ar), 1611vs (C=N), and 1579sh (C=C). MS (EI, 220 °C): *m*/*z* (%) = 650 (7) [M = $Zn(S1)_2]^+$, 545 (2) [M–CH$(CH_3)(C_6H_5)]^+$, 476 (4) [M–CH$(CH_3)(C_6H_5)$–2Cl + H]$^+$, 358 (5) [Zn(*S*1)]$^+$, 292 (20) [*S*-H1−H]$^+$, 189 (15) [$C_6H_2(Cl_2)$(CHNH)(OH)]$^+$, 105 (100) [C_6H_5(CHNH)]$^+$ and 77 (15) [$C_6H_5]^+$ {*S*-H1 = $C_{15}H_{12}Cl_2NOH$ = (*S*)-*N*-1-(phenyl)ethyl-2,4-Cl,Cl-salicylaldimine}. Anal. calc. for $C_{30}H_{24}Cl_4ZnN_2O_2$: C, 55.29; H, 3.71; N, 4.30%. Found: C, 55.30; H, 3.71; N, 4.31%.

Bis[(*R*)-*N*-1-(phenyl)ethyl-2,4-Br,Br-salicylaldiminato-κ^{2}N,O]-zinc(II), (Zn*R*2). Yield: 89%. IR (KBr, cm^{-1}): ν = 3054, 3033, 2974, 2935w (H–Ar), 1610vs (C=N), and 1575s (C=C). MS (EI, 240 °C): *m*/*z* (%) = 830 (2) [M = $Zn(R2)_2]^+$, 446 (2) [Zn(*R*2)]$^+$, 383 (9) [*R*-H2]$^+$, 279 (12) [$C_6H_2(Br_2)$(CHNH)(OH)]$^+$, 105 (100) [C_6H_5(CHNH)]$^+$ and 77 (15) [$C_6H_5]^+$ {*R*-H2 = $C_{15}H_{12}Br_2NOH$ = (*R*)-*N*-1-(phenyl)ethyl-2,4-Br,Br-salicylaldimine}. Anal. calc. for $C_{30}H_{24}Br_4ZnN_2O_2$: C, 43.44; H, 2.92; N, 3.38%. Found: C, 43.41; H, 2.94; N, 3.41%.

Bis[(*S*)-*N*-1-(phenyl)ethyl-2,4-Br,Br-salicylaldiminato-κ^{2}N,O]-zinc(II), (Zn*S*2). Yield: 85%. ν = 3053, 3033, 2974, 2934w (H–Ar), 1609vs (C=N), and 1575s (C=C). MS (EI, 230 °C): *m*/*z* (%) = 830 (3) [M = $Zn(S2)_2]^+$, 446 (3) [Zn(*S*2)]$^+$, 383 (9) [*S*-H2]$^+$, 279 (12) [$C_6H_2(Br_2)$(CHNH)(OH)]$^+$, 105 (100) [C_6H_5(CHNH)]$^+$ and 77 (15) [$C_6H_5]^+$ {*S*-H2 = $C_{15}H_{12}Br_2NOH$ = (*S*)-*N*-1-(phenyl)ethyl-2,4-Br,Br-salicylaldimine}. Anal. calc. for $C_{30}H_{24}Br_4ZnN_2O_2$: C, 43.44; H, 2.92; N, 3.38%. Found: C, 43.45; H, 2.95; N, 3.43%.

Bis[(*R*)-*N*-1-(phenyl)ethyl-2,4-Cl,Br-salicylaldiminato-κ^{2}N,O]-zinc(II), (Zn*R*3). Yield: 86%. ν = 3057, 3033, 2977, 2936w (H–Ar), 1610vs (C=N), and 1584s (C=C). MS (EI, 220 °C): *m*/*z* (%) = 740 (2) [M = $Zn(R3)_2]^+$, 402 (2) [Zn(*R*3)]$^+$, 339 (11) [*R*-H3]$^+$, 235 (13) [C_6H_2(Cl)(Br)(CHNH)(OH)]$^+$, 105 (100) [C_6H_5(CHNH)]$^+$ and 77 (13) [$C_6H_5]^+$ {*R*-H3 = $C_{15}H_{12}ClBrNOH$ = (*R*)-*N*-1-(phenyl) ethyl-2,4-Cl,Br-salicylaldimine}. Anal. calc. for $C_{30}H_{24}Cl_2Br_2ZnN_2O_2$: C, 48.65; H, 3.27; N, 3.78%. Found: C, 48.65; H, 3.28; N, 3.80%.

Bis[(*S*)-*N*-1-(phenyl)ethyl-2,4-Cl,Br-salicylaldiminato-κ^{2}N,O]-zinc(II), (Zn*S*3). Yield: 87%. ν = 3057, 3033, 2977, 2936w (H–Ar), 1610vs (C=N), and 1583s (C=C). MS (EI, 240 °C): *m*/*z* (%) = 740 (6) [M = $Zn(S3)_2]^+$, 402 (5) [Zn(*S*3)]$^+$, 339 (10) [*S*-H3]$^+$, 235 (10) [C_6H_2(Cl)(Br)(CHNH)(OH)]$^+$, 105 (100) [C_6H_5(CHNH)]$^+$ and 77 (12) [$C_6H_5]^+$ {*S*-H3 = $C_{15}H_{12}ClBrNOH$ = (*S*)-*N*-1-(phenyl) ethyl-2,4-Cl,Br-salicylaldimine}. Anal. calc. for $C_{30}H_{24}Cl_2Br_2ZnN_2O_2$: C, 48.65; H, 3.27; N, 3.78%. Found: C, 48.67; H, 3.27; N, 3.78%.

X-ray crystallography

Single-crystal X-ray diffraction data for all Zn(II)-Schiff base complexes except Δ-Zn*S*3 were collected at 160(1) K on a Rigaku OD XtaLAB Synergy, Dualflex, Pilatus 200 K diffractometer using a single wavelength X-ray source (Mo K_α radiation: λ = 0.71073 Å) from a micro-focus sealed X-ray tube and an Oxford liquid-nitrogen Cryostream cooler. X-ray diffraction data for Δ-Zn*S*3 were collected at 160(1) K on a Rigaku OD SuperNova/Atlas area-detector diffractometer using Cu K_α radiation (λ = 1.54184 Å) from a micro-focus X-ray source and an Oxford Instruments Cryojet XL cooler. The selected suitable single crystal was mounted using polybutene oil on a flexible loop fixed on a goniometer head and immediately transferred to the diffractometer. Pre-experiment, data collection, data reduction and analytical absorption correction[60] were performed with the program suite *CrysAlisPro*[61] using *Olex2*,[62] and the structure was solved with the *SHELXT*[63] small molecule structure solution program and refined with the *SHELXL2018/3* program package[64] by full-matrix least-squares minimization on F^2. Hydrogen atoms were placed in the calculated positions by means of the "riding" model. *PLATON*[65] was used to check the result of the X-ray analysis. More details concerning the crystal structures and refinements can be found in Table S1† or in the corresponding CIF files.

CCDC 2000646, 2000644, 2000648, 2000652, 2000650 and 2000653† contain the supplementary crystallographic data for Λ-Zn*R*1–3/Δ-Zn*S*1–3, respectively.

Computational section

A thorough computational procedure was performed with Gaussian 09[66] to justify the experimental results, and hence to gain detailed insight into the electronic/chiroptical properties associated with diastereoselection and Δ *vs.* Λ-chirality induction at-metal center. The transition metal(II)-complexes with chiral Schiff base ligands in a tetrahedral or pseudotetrahedral geometry exhibit induced chirality-at-metal, and thereby give oppositely configured two diastereomers (*e.g.*, Δ-M and Λ-M) along the C_2-symmetry of the molecule.[29–32,35–38] Therefore, we optimized both the diastereomers for all three pairs of complexes Δ-Zn*R*1/Λ-Zn*R*1 and Δ-Zn*S*1/Λ-Zn*S*1; Δ-Zn*R*2/Λ-Zn*R*2 and Δ-Zn*S*2/Λ-Zn*S*2; Δ-Zn*R*3/Λ-Zn*R*3 and Δ-Zn*S*3/Λ-Zn*S*3 at b3lyp/6-31g(d), respectively (Fig. S10†). For optimization, the initial gas phase geometries for the diastereomers Λ-Zn*R*1, Δ-Zn*S*1, Λ-Zn*R*2, Δ-Zn*S*2, Λ-Zn*R*3 and Δ-Zn*S*3 were generated from their single crystal X-ray structures, respectively. The geometries with the opposite configuration at-metal center such as Δ-Zn*R*1, Λ-Zn*S*1, Δ-Zn*R*2, Λ-Zn*S*2, Δ-Zn*R*3 and Λ-Zn*S*3 were built by mirror inversion of the corresponding diastereomer followed by manual inversion of the chiral-carbon center.[29–32] The optimizations were performed allowing all bonds and angles freely rotatable around the metal centre and in the whole structure.

The excited state properties (UV-Vis and ECD spectra) by DFT/TD-DFT were analysed with different combinations of the functionals including cam-b3lyp, b3lyp and m06 and the basis sets tzvp and sdd, respectively for Δ-Zn*S*1 (Fig. S11 and S12†). The results provide almost identical spectra with little shifting of the bands' maxima, strongly supporting the reliability and validity of the methods used. However, the best fit to the experimental spectra was obtained at the b3lyp/tzvp//b3lyp/6-31g(d) level of theory. For this reason, the excited state properties for the remaining diastereomers (Λ-Zn*S*1, Δ-Zn*R*1/Λ-Zn*R*1, Δ-Zn*S*2/Λ-Zn*S*2, Δ-Zn*R*2/Λ-Zn*R*2, Δ-Zn*R*3/Λ-Zn*R*3 and Δ-Zn*S*3/Λ-Zn*S*3) were analysed only with b3lyp/tzvp//b3lyp/6-31g(d), respectively. The PCM (polarization continuum model) was incorporated using chloroform as the solvent and the 72 excited states (roots) were considered for calculations. The simulated UV-Vis and ECD spectra were generated using the program SpecDis[67] by applying the Gaussian band shape with exponential half-width σ = 0.16 eV. The ^{1}H NMR spectra were computed at GIAO B3LYP/6-311+G(2d,p) with the PCM in dmso for the diastereomeric pairs Δ/Λ-Zn*S*1 and Λ/Δ-Zn*R*1 using the corresponding optimized structures at b3lyp/6-31G(d), respectively. Assessments of the Δ- and Λ-diastereomers were made following the computed ^{1}H NMR spectra and found to be in good accord with the experimental spectra.

Authors contributions

All co-authors have agreed to submit the manuscript for publication and accept the responsibility for including their names as co-authors.

Conflicts of interest

There are no conflicts of interest to declare.

Acknowledgements

The authors are grateful to the Research Council of the University of Isfahan (Iran) for financial support of this work. We acknowledge the financial support from the Alexander von Humboldt Foundation (AvH), Bonn, Germany under the project "Research Group Linkage Program". We recognize the "Wazed Miah Science Research Centre" at Jahangirnagar University, Dhaka, Bangladesh. We thank Professor ABP Lever, Department of Chemistry, York University, Toronto and the computecanada.ca (https://ccdb.computecanada.ca/) Ontario, Canada, for using computational resources.

References

1 H. Amouri and M. Gruselle, *Chirality in Transition Metal Chemistry: Molecules, supramolecular assemblies and materials*, John Wiley & Sons, Chichester, 2008.
2 A. von Zelewsky, *Stereochemistry of Coordination Compounds*, John Wiley & Sons, Chichester, 1996.
3 E. C. Constable, *Chem. Soc. Rev.*, 2013, **42**, 1637.
4 R. E. Ernst, M. J. O'Connor and R. H. Holm, *J. Am. Chem. Soc.*, 1967, **89**, 6104.
5 T. Ohno, S. Chorazy, K. Imoto and S. Ohkoshi, *Cryst. Growth Des.*, 2016, **16**, 4119.
6 A. von Zelewsky and O. Mamula, *J. Chem. Soc., Dalton Trans.*, 2000, 219.
7 E. C. Constable, G. Zhang, C. E. Housecroft, M. Neuburger and J. A. Zampese, *Chem. Commun.*, 2010, 3077.
8 E. C. Constable, C. E. Housecroft, T. Kulke, C. Lazzarini, E. R. Schofield and Y. Zimmermann, *Chem. Soc., Dalton Trans.*, 2001, 2864.
9 S. E. Howson, L. E. Allan, N. P. Chmel, G. J. Clarkson, R. van Gorkum and P. Scott, *Chem. Commun.*, 2009, 1727.
10 J. M. Becker, J. Barker, G. J. Clarkson, R. van Gorkum, G. K. Johal, R. I. Walton and P. Scott, *Dalton Trans.*, 2010, **39**, 2309.
11 K. A. Jensen, *Inorg. Chem.*, 1970, **9**, 1.
12 U. Knof and A. von Zelewsky, *Angew. Chem., Int. Ed.*, 1999, **38**, 302.
13 O. Mamula, A. von Zelewsky, T. Bark, H. Stoeckli-Evans, A. Neels and G. Bernardinelli, *Chem. – Eur. J.*, 2000, **6**, 3575.
14 H. Song, M. Postings, P. Scott and N. J. Rogers, *Chem. Sci.*, 2021, **12**, 1620.
15 H. Brunner, M. Niemetz and M. Zabel, *Z. Naturforsch., B: J. Chem. Sci.*, 2000, **55**, 145.
16 C. Evans and D. Luneau, *J. Chem. Soc., Dalton Trans.*, 2002, 83.
17 G. Brewer, C. Brewer, R. J. Butcher, G. T. Robichaux and C. Viragh, *Inorg. Chim. Acta*, 2014, **410**, 171.

18 H. Sakiyama, H. Okawa, N. Matsumoto and S. Kida, *Bull. Chem. Soc. Jpn.*, 1991, **64**, 2644.
19 H. Sakiyama, H. Okawa, N. Matsumoto and S. Kida, *J. Chem. Soc., Dalton Trans.*, 1990, 2935.
20 T. Akitsu, *Polyhedron*, 2007, **26**, 2527.
21 Z. Dezhahang, M. R. Poopari, J. Cheramy and Y. J. Xu, *Inorg. Chem.*, 2015, **54**, 4539.
22 H. Ōkawa, M. Nakamura and S. Kida, *Inorg. Chim. Acta*, 1986, **120**, 185.
23 T. Akitsu and Y. Einaga, *Polyhedron*, 2005, **24**, 2933.
24 T. Akitsu and Y. Einaga, *Acta Crystallogr., Sect. C: Cryst. Struct. Commun.*, 2004, **60**, m640.
25 M. Górecki, M. Enamullah, M. A. Islam, M. K. Islam, S.-P. Höfert, D. Woschko, C. Janiak and G. Pescitelli, *Inorg. Chem.*, 2021, **60**, 14116.
26 M. Enamullah, V. Vasylyeva, M. A. Quddus, M. K. Islam, S. P. Höfert and C. Janiak, *CrystEngComm*, 2018, **20**, 4724.
27 M. Enamullah, M. A. Quddus, M. M. Rahman and T. E. Burrow, *J. Mol. Struct.*, 2017, **1130**, 765.
28 M. Enamullah, M. A. Islam, B. A. Joy, B. Dittrich, G. J. Reiss and C. Janiak, *Inorg. Chim. Acta*, 2018, **482**, 935.
29 M. Enamullah, G. Makhloufi, R. Ahmed, B. Alif Joy, M. A. Islam, D. Padula, H. Hunter, G. Pescitelli and C. Janiak, *Inorg. Chem.*, 2016, **55**, 6449.
30 M. Enamullah, A. K. M. Royhan Uddin, G. Pescitelli, R. Berardozzi, G. Makhloufi, V. Vasylyeva, A.-C. Chamayou and C. Janiak, *Dalton Trans.*, 2014, **43**, 3313.
31 M. Enamullah, M. A. Quddus, M. R. Hasan, G. Pescitelli, R. Berardozzi, G. Makhloufi, V. Vasylyeva and C. Janiak, *Dalton Trans.*, 2016, **45**, 667.
32 G. Pescitelli, S. Lüdeke, A.-C. Chamayou, M. Marolt, V. Justus, M. Górecki, L. Arrico, L. Di Bari, M. A. Islam, I. Gruber, M. Enamullah and C. Janiak, *Inorg. Chem.*, 2018, **57**, 13397.
33 M. Enamullah, V. Vasylyeva and C. Janiak, *Inorg. Chim. Acta*, 2013, **408**, 109.
34 M. Enamullah, M. A. Quddus, M. R. Hasan, G. Pescitelli, R. Berardozzi, G. J. Reiß and C. Janiak, *Eur. J. Inorg. Chem.*, 2015, **2015**, 2758.
35 M. Enamullah, M. Anwar, M. K. Islam, D. Woschko and C. Janiak, *Dalton Trans.*, 2021, **50**, 9236.
36 A.-C. Chamayou, G. Makhloufi, L. A. Nafie, C. Janiak and S. Lüdeke, *Inorg. Chem.*, 2015, **54**, 2193.
37 A.-C. Chamayou, S. Lüdeke, V. Brecht, T. B. Freedman, L. A. Nafie and C. Janiak, *Inorg. Chem.*, 2011, **50**, 11363.
38 N. Kordestani, H. A. Rudbari, G. Bruno, S. Rosario, J. D. Braun, D. E. Herbert, O. Blacque, I. Correia, M. A1-M Zaman, M. M. Bindu, C. Janiak and M. Enamullah, *Dalton Trans.*, 2020, **49**, 8247.
39 C. Merten, R. McDonald and Y. Xu, *Inorg. Chem.*, 2014, **53**, 3177.
40 M. Albrecht, E. Isaak, M. Baumert, V. Gossen, G. Raabe and R. Fröhlich, *Angew. Chem., Int. Ed.*, 2011, **50**, 2850.
41 C. M. Álvarez, R. Carrillo, R. García-Rodríguez and D. Miguel, *Chem. Commun.*, 2011, **47**, 12765.
42 J. Gregoliński, M. Hikita, T. Sakamoto, H. Sugimoto, H. Tsukube and H. Miyake, *Inorg. Chem.*, 2016, **55**, 633.
43 S. Zahn and J. W. Canary, *Science*, 2000, **288**, 1404.
44 J. Jacques, A. Collet and S. H. Wilen, *Enantiomers, Racemates, and Resolution*, Krieger Publishing, Melbourne, FL, 1994.
45 M. Enamullah, A. Uddin, A. C. Chamayou and C. Janiak, *Z. Naturforsch., B: J. Chem. Sci.*, 2007, **62**, 807.
46 M. Enamullah, A. R. Uddin, G. Hogarth and C. Janiak, *Inorg. Chim. Acta*, 2012, **387**, 173.
47 H. D. Flack, M. Sadki, A. L. Thompson and D. J. Watkin, *Acta Crystallogr., Sect. A: Fundam. Crystallogr.*, 2011, **67**, 21.
48 H. D. Flack and G. Bernardinelli, *Chirality*, 2008, **20**, 681.
49 H. D. Flack and G. Bernardinelli, *Acta Crystallogr., Sect. A: Fundam. Crystallogr.*, 1999, **55**, 908.
50 H. Flack, *Acta Crystallogr., Sect. A: Fundam. Crystallogr.*, 1983, **39**, 876.
51 Y. Shibuya, K. Nabari, M. Kondo, S. Yasue, K. Maeda, F. Uchida and H. Kawaguchi, *Chem. Lett.*, 2008, **37**, 78.
52 L. Yang, D. R. Powell and R. P. Houser, *Dalton Trans.*, 2007, 955.
53 A. V. Bondi, *J. Phys. Chem.*, 1964, **68**, 441.
54 O. V. Shishkin, *Chem. Phys. Lett.*, 2008, **458**, 96.
55 (*a*) M. J. Turner, J. J. McKinnon, S. K. Wolff, D. J. Grimwood, P. R. Spackman, D. Jayatilaka and M. A. Spackman, *CrystalExplorer 17*, University of Western Australia, 2017, http://hirshfeldsurface.net; (*b*) J. J. McKinnon, M. A. Spackman and A. S. Mitchell, *Acta Crystallogr., Sect. B: Struct. Sci.*, 2004, **60**, 627; (*c*) M. A. Spackman and J. J. McKinnon, *CrystEngComm*, 2002, **4**, 378; (*d*) J. J. McKinnon, D. Jayatilaka and M. A. Spackman, *Chem. Commun.*, 2007, 3814; (*e*) P. R. Spackman, M. J. Turner, J. J. McKinnon, S. K. Wolff, D. J. Grimwood, D. Jayatilaka and M. A. Spackman, *J. Appl. Crystallogr.*, 2021, **54**, 1006.
56 C. Lefebvre, G. Rubez, H. Khartabil, J.-C. Boisson, J. Contreras-García and E. Hénon, Accurately extracting the signature of intermolecular interactions present in the NCI plot of the reduced density gradient versus electron density, *Phys. Chem. Chem. Phys.*, 2017, **19**, 17928.
57 T. Lu and F. Chen, Multiwfn: A Multifunctional Wavefunction Analyzer, *J. Comput. Chem.*, 2012, **33**, 580.
58 J. Klein, H. Khartabil, J.-C. Boisson, J. Contreras-García, J.-P. Piquemal and E. Hénon, New Way for Probing Bond Strength, *J. Phys. Chem. A*, 2020, **124**, 1850.
59 C. F. Macrae, I. Sovago, S. J. Cottrell, P. T. A. Galek, P. McCabe, E. Pidcock, M. Platings, G. P. Shields, J. S. Stevens, M. Towler and P. A. Wood, *J. Appl. Crystallogr.*, 2020, **53**, 226.
60 R. C. Clark and J. S. Reid, *Acta Crystallogr., Sect. A: Fundam. Crystallogr.*, 1995, **51**, 887.
61 *CrysAlisPro, Rigaku Oxford Diffraction, release 1.171.40.53*, 2019.
62 O. V. Dolomanov, L. J. Bourhis, R. J. Gildea, J. A. Howard and H. Puschmann, *J. Appl. Crystallogr.*, 2009, **42**, 339.

63 G. M. Sheldrick, SHELXT – Integrated space-group and crystal-structure determination, *Acta Crystallogr., Sect. A: Found. Adv.*, 2015, **71**, 3.
64 G. M. Sheldrick, SHELXL – Crystal structure refinement, *Acta Crystallogr., Sect. C: Struct. Chem.*, 2015, **71**, 3.
65 A. L. Spek, *Acta Crystallogr., Sect. D: Biol. Crystallogr.*, 2009, **65**, 148.
66 M. J. Frisch, G. W. Trucks, H. B. Schlegel, G. E. Scuseria, M. A. Robb, J. R. Cheeseman, G. Scalmani, V. Barone, B. Mennucci, G. A. Petersson, H. Nakatsuji, M. Caricato, X. Li, H. P. Hratchian, A. F. Izmaylov, J. Bloino, G. Zheng, J. L. Sonnenberg, M. Hada, M. Ehara, K. Toyota, R. Fukuda, J. Hasegawa, M. Ishida, T. Nakajima, Y. Honda, O. Kitao, H. Nakai, T. Vreven, J. A. Montgomery Jr., J. E. Peralta, F. Ogliaro, M. Bearpark, J. J. Heyd, E. Brothers, K. N. Kudin, V. N. Staroverov, R. Kobayashi, J. Normand, K. Raghavachari, A. Rendell, J. C. Burant, S. S. Iyengar, J. Tomasi, M. Cossi, N. Rega, J. M. Millam, M. Klene, J. E. Knox, J. B. Cross, V. Bakken, C. Adamo, J. Jaramillo, R. Gomperts, R. E. Stratmann, O. Yazyev, A. J. Austin, R. Cammi, C. Pomelli, J. W. Ochterski, R. L. Martin, K. Morokuma, V. G. Zakrzewski, G. A. Voth, P. Salvador, J. J. Dannenberg, S. Dapprich, A. D. Daniels, Ö. Farkas, J. B. Foresman, J. V. Ortiz, J. Cioslowski and D. J. Fox, *Gaussian 09, Revision D.01*, Gaussian, Inc., Wallingford CT, 2009.
67 T. Bruhn, A. Schaumlöffel, Y. Hemberger and G. Bringmann, *Chirality*, 2013, **25**, 243.